THE ASTROPHYSICAL JOURNAL, 219:705–726, 1978 January 15

BACKSCATTER, ANISOTROPY, AND POLARIZATION OF SOLAR HARD X-RAYS

T. BAI* AND R. RAMATY
Laboratory for High Energy Astrophysics, NASA/Goddard Space Flight Center
Received 1977 January 13; accepted 1977 July 7

ABSTRACT

Hard X-rays incident upon the photosphere with energies $\gtrsim 15$ keV have high probabilities of backscatter due to Compton collisions with electrons. This effect has a strong influence on the spectrum, intensity, and polarization of solar hard X-rays—especially for anisotropic models in which the primary X-rays are emitted predominantly toward the photosphere. We have carried out a detailed study of X-ray backscatter, and we have investigated the interrelated problems of anisotropy, polarization, center-to-limb variation of the X-ray spectrum, and Compton backscatter in a coherent fashion. The results of this study are compared with observational data. Because of the large contribution from the backscatter, for an anisotropic primary X-ray source which is due to bremsstrahlung of accelerated electrons moving predominantly down toward the photosphere, the observed X-ray flux around 30 keV does not depend significantly on the position of flare on the Sun. For such an anisotropic source, the X-ray spectrum observed in the 15–50 keV range becomes steeper with the increasing heliocentric angle of the flare. These results are compatible with the data. The degree of polarization of the sum of the primary and reflected X-rays with energies between about 15 and 30 keV can be very large for anisotropic primary X-ray sources, but it is less than about 4% for isotropic sources. We also discuss the characteristics of the brightness distribution of the X-ray albedo patch created by the Compton backscatter. The height and anisotropy of the primary hard X-ray source might be inferred from the study of the albedo patch.

Subject headings: polarization — Sun: flares — Sun: X-rays

I. INTRODUCTION

Because bremsstrahlung is directional and polarized, the study of the directionality of solar hard X-rays and/or the study of their polarization can lead to the knowledge on the angular distribution of accelerated electrons in the emitting region. Such knowledge is essential in determining whether hard X-rays are due to thermal or nonthermal electrons and in understanding the acceleration mechanisms. Several authors have studied the anisotropy and polarization of solar hard X-rays. Brown (1972) and Petrosian (1973) studied the anisotropy, and Elwert and Haug (1970), Haug (1972), and Brown (1972) studied polarization. Kane (1974), Datlowe, Elcan, and Hudson (1974), and Datlowe *et al.* (1977) analyzed the OGO-5 and OSO-7 data, respectively, to find out the effects of the anisotropy (center-to-limb variations). Tindo and his co-workers (Tindo *et al.* 1970, 1972*a*, *b*; Tindo, Mandel'stam, and Suryghin 1973) measured the polarization of solar hard X-rays.

However, as pointed out by Tomblin (1972) and by Santangelo, Horstman, and Horstman-Moretti (1973), photons in the energy range 10–100 keV, when emitted down toward the photosphere, have a high probability of being reflected due to Compton scattering. As a result of this reflection, both the spectrum and the intensity of the X-rays are significantly modified, especially for anisotropic X-ray sources which radiate predominantly in the downward direction. Furthermore, because the Compton scattering cross section is dependent on the polarization of the photon beam, the reflectivity depends on the polarization, and the backscattered photon component influences the degree of polarization of the observed photons. Therefore, the backscatter, polarization, and anisotropy of solar hard X-rays should be studied together in a coherent fashion.

Until recently, however, the effect of the Compton backscatter was not taken into account in the studies of the anisotropy and the polarization of solar hard X-rays (Elwert and Haug 1970; Haug 1972; Brown 1972; Petrosian 1973), nor was the effect of the anisotropy (and the polarization) of the primary photon source taken into consideration in the study of the backscatter (Santangelo, Horstman, and Horstman-Moretti 1973). Recently, Henoux (1975) considered the effect of the Compton backscatter on the anisotropy and the polarization of solar hard X-rays. However, he used somewhat unrealistic anisotropic models in which electrons are spiraling down with given pitch angles 0°, 60°, and 90° for each case. We have recently learned, while this paper was being revised, that Langer and Petrosian (1977) have also treated a similar problem for beams of electrons directed vertically down toward the photosphere.

As discussed above, the Compton backscatter complicates the relationships between the anisotropy and the polarization of hard X-rays and the anisotropy of the accelerated electrons. This backscatter, however, may give

* Also University of Maryland, Department of Physics and Astronomy. Research supported by NASA grant 21-002-316.

extra information by reflecting the photons incident on the photosphere which could not be observed otherwise. If the size of the primary X-ray source is considerably smaller than its height, then in principle the primary source can be resolved from its albedo. When such resolution is possible, three independent measurements can give information on the height of the primary source and the anisotropy. These are the ratio between the number of primary X-rays and the number of reflected X-rays, the distribution of surface brightness of the albedo patch (the bright area on the photosphere from which X-rays are reflected), and, if the primary source is not at the disk center, the displacement of the projection of the source with respect to the centroid of the albedo patch. Brown, van Beek, and McClymont (1975) discussed the possibility of determining the height of the primary X-ray source from the size of the albedo patch. It is anticipated that such measurements could be performed by the Hard X-ray Imaging Spectrometer which will be included in the payload of NASA's Solar Maximum Mission. In their calculations, however, Brown, van Beek, and McClymont (1975) assumed that the reflection probability is independent of the incident direction of the photon—and this assumption is not valid in general.

As mentioned above, the effects of the backscatter on the polarization and anisotropy have been studied by Henoux (1975) and Langer and Petrosian (1977). However, they considered only anisotropic cases in each of which accelerated electrons have a given pitch angle without any angular dispersion of electron momentum vectors. In this paper we present a coherent study of the interrelated problem of the Compton backscatter, anisotropy, and polarization of solar hard X-rays. For anisotropic sources we realistically allow the accelerated electrons to have angular dispersions of momentum vectors, and we also consider isotropic sources with power-law and thermal spectra. By doing so, we study the effects of anisotropic electron distributions and Compton backscatter on the anisotropy and polarization of hard X-rays in detail. By investigating the differential reflectivity of X-rays as a function of incident and outgoing photon directions, we also study the characteristics of the albedo brightness distribution.

In § II we review the methods of representing the state of polarization by Stokes parameters and of expressing the Compton scattering cross section in a matrix form. We further describe the Monte Carlo simulation used in this paper. In § III we present the results of our Monte Carlo simulations for isotropic as well as anisotropic (polarized) primary sources. Here we also discuss the directivity of the sum of photons due to the primary source and those due to the backscatter. We also discuss the characteristics of the energy spectra of the resultant hard X-rays, and compare the results with the observed OSO-7 data (Datlowe, Elcan, and Hudson 1974).

In § IV, by taking the effect of Compton backscatter into account, we study the polarization of solar hard X-rays due to isotropic, unpolarized, as well as anisotropic, polarized primary sources. In § V, by calculating the differential reflectivity of a beam of photons for various incident angles, we study in detail the characteristics of the albedo patch, which is a bright X-ray patch on the photosphere created by the Compton backscatter. Information on the height of the primary source, the anisotropy, and polarization of primary hard X-rays might be obtained from detailed albedo measurements. In § VI we summarize our results and compare with other researchers' theoretical and observational results.

II. METHODS OF CALCULATIONS

a) The Stokes Parameters and the Matrix Representation of the Compton Scattering Cross Section

Hard X-rays released down to the photosphere are either Compton scattered or absorbed by the photoelectric effect. The differential Compton cross section is given by (Klein and Nishina 1929)

$$\frac{d\sigma_c}{d\Omega}(\epsilon_0, \theta_s, \Theta) = \tfrac{1}{4} r_0^2 \left(\frac{\epsilon}{\epsilon_0}\right)^2 \left(\frac{\epsilon_0}{\epsilon} + \frac{\epsilon}{\epsilon_0} - 2 + 4\cos^2\Theta\right). \tag{1}$$

Here θ_s is the scattering angle, Θ is the angle between the directions of polarization of the initial photon and the final photon, $r_0 = 2.82 \times 10^{-13}$ cm, and ϵ_0 and ϵ are the initial and final photon energies related by

$$\epsilon = \epsilon_0/[1 + (\epsilon_0/mc^2)(1 - \cos\theta_s)], \tag{2}$$

where mc^2 is the electron rest mass energy.

The formula given by equation (1) is applicable only to a coherent beam with plane polarization or to a beam of photons whose exact distribution of polarization vectors is known. To deal with a beam of photons with an arbitrary distribution of polarization vectors, it is more advantageous to use the Stokes parameters, because they are directly measurable quantities and are additive for independent (noncoherent) emission fluxes. In the application of the Stokes parameters to a Compton scattering problem, it is convenient to write them in the form of a four-vector and to use the matrix representation of the Compton cross section. The matrix representation of the Compton cross section has been well reviewed by McMaster (1961). Henoux (1975) used Stokes parameters and the matrix representation of the Compton cross section.

The Stokes parameters are represented by a four-vector,

$$\begin{pmatrix} I \\ P_1 \\ P_2 \\ P_3 \end{pmatrix} = \begin{pmatrix} I \\ \boldsymbol{P} \end{pmatrix}. \tag{3}$$

Here I represents the beam intensity and is normalized to 1 throughout in this paper; $P_1 = (I_\perp - I_\parallel)/I$ represents the degree of polarization measured with respect to a given reference plane; P_2 represents the degree of polarization measured with respect to a plane rotated around the direction of the propagation by 45° from the reference plane; and P_3 represents the state of circular polarization. For example, col. (1, 0, 0, 0) represents an unpolarized beam, col. (1, ±1, 0, 0) represents plane polarization perpendicular (parallel) to the reference plane, col. (1, 0, ±1, 0) represents plane polarization perpendicular (parallel) to the plane obtained by rotating the reference plane by 45°, and col. (1, 0, 0, ±1) represents left (right) circular polarization. Since photons with circular polarization carry angular momentum, bremsstrahlung photons produced by unpolarized electrons have no circular polarization. Since we consider only unpolarized electron beams, we neglect circular polarization in this paper. The Stokes parameters can therefore be written as a three-vector, col. $(1, P_1, P_2)$.

Since the Stokes parameters are coordinate dependent, there exists a rotation matrix **M** for the Stokes parameters (McMaster 1961):

$$\mathbf{M} = \begin{pmatrix} 1 & 0 & 0 \\ 0 & \cos 2\phi & \sin 2\phi \\ 0 & -\sin 2\phi & \cos 2\phi \end{pmatrix}, \tag{4}$$

where ϕ is the angle of rotation around the direction of the propagation. Note that **M** is a unit matrix when $\phi = \pi$, as it should be.

The matrix representation of the Klein-Nishina formula is given by (McMaster 1961)

$$\mathbf{T} = \tfrac{1}{2} r_0^2 \left(\frac{\epsilon^2}{\epsilon_0}\right) \begin{pmatrix} \epsilon_0/\epsilon + \epsilon/\epsilon_0 - \sin^2\theta_s & \sin^2\theta_s & 0 \\ \sin^2\theta_s & 1 + \cos^2\theta_s & 0 \\ 0 & 0 & \cos 2\theta_s \end{pmatrix}. \tag{5}$$

This matrix gives the relationship between the Stokes parameters before the scattering and the Stokes parameters after the scattering, where the Stokes parameters are specified with respect to the scattering plane. However, the scattering plane is not a unique plane to be used as a reference plane. If the distribution of the accelerated electrons (and consequently that of the hard X-rays) is symmetric around the normal to the photosphere, the plane containing the normal and the direction of the photon propagation defines a unique plane, with respect to which we can calculate the Stokes parameters of the photon flux propagating along that direction. Because this plane is normal to the photosphere, let us call it the *normal plane* hereafter. The Stokes parameters with respect to the normal plane after the scattering are obtained by applying appropriate rotation matrices and equation (5). (For a more detailed discussion on this, see Bai 1977.)

The Compton scattering cross section for a polarized beam is given by

$$\begin{aligned} \frac{d\sigma}{d\Omega}(\theta_s, \phi_s) &= (1 \quad 0 \quad 0)\mathbf{T} \begin{pmatrix} 1 & 0 & 0 \\ 0 & \cos 2\phi_s & \sin 2\phi_s \\ 0 & -\sin 2\phi_s & \cos 2\phi_s \end{pmatrix} \begin{pmatrix} 1 \\ P_1 \\ P_2 \end{pmatrix} \\ &= \tfrac{1}{2} r_0^2 \left(\frac{\epsilon}{\epsilon_0}\right)^2 \left\{ \frac{\epsilon}{\epsilon_0} + \frac{\epsilon_0}{\epsilon} - \sin^2\theta_s (1 - P_1 \cos 2\phi_s - P_2 \sin 2\phi_s) \right\}, \end{aligned} \tag{6}$$

where ϕ_s is the angle between the scattering plane and the reference plane for the Stokes parameters. For an unpolarized beam, this formula becomes

$$\frac{d\sigma_c}{d\Omega}(\epsilon_0, \theta_s) = \tfrac{1}{2} r_0^2 \left\{ \left(\frac{\epsilon}{\epsilon_0}\right)^3 + \frac{\epsilon}{\epsilon_0} - \left(\frac{\epsilon}{\epsilon_0}\right)^2 \sin^2\theta_s \right\}. \tag{7}$$

This cross-section formula is also the same as equation (6) averaged over ϕ_s. The total Compton cross section is

$$\sigma_c(\epsilon_0) = 2\pi r_0^2 \left\{ \frac{1+\alpha}{\alpha^2} \left[\frac{2(1+\alpha)}{1+2\alpha} - \frac{\ln(1+2\alpha)}{\alpha} \right] + \frac{\ln(1+2\alpha)}{2\alpha} - \frac{1+3\alpha}{(1+2\alpha)^2} \right\}, \tag{8}$$

where $\alpha = \epsilon_0/mc^2$. In our calculation we multiply this cross section by 1.15 to take into account the effects of He and heavier elements.

We use the photoelectric absorption cross section, σ_a, given by Fireman (1974). At the energies of interest ($\gtrsim 10$ keV), this cross section depends mainly on the abundance of heavy elements such as O, Fe, and Ni. Fireman

(1974) used the photospheric abundances given by Withbroe (1971). The following analytical form is a good approximation to the extrapolation of his result to energies $\gtrsim 10$ keV:

$$\sigma_a(\epsilon_0) = 7.2 \times 10^{-22}\epsilon_0^{-2.78}(\text{cm}^2 \text{ per H-atom}), \tag{9}$$

where ϵ_0 is in keV. This cross section asymptotically approaches to the form ϵ_0^{-3} as energy increases; however, equation (9) is a better approximation in the regime where the absorption is important. At 12.5 keV the absorption cross section and the Compton cross section are equal to each other.

b) Calculation of the Stokes Parameters of the Bremsstrahlung Hard X-Rays due to Anisotropic Electrons

As we have seen, the Compton cross section depends on the degree of polarization. Therefore, to calculate the backscatter, we need to know the degree of polarization of primary hard X-rays and to follow the polarization throughout the scattering process. Because for the integral reflectivity the azimuthal dependence of the Compton cross section given by equation (6) is averaged over various incident and outgoing directions, the integral reflectivity is not much affected by neglecting the polarization dependence. However, the angular dependence of the reflectivity (the differential reflectivity) and especially the albedo brightness distribution are expected to be affected by the polarization dependence of the Compton cross section.

The degree of polarization of bremsstrahlung due to a beam of monoenergetic electrons is given by

$$P_1(\epsilon, \theta) = \left[\frac{d^2\sigma_\perp(E, \epsilon, \theta)}{d\epsilon d\Omega} - \frac{d^2\sigma_\parallel(E, \epsilon, 0)}{d\epsilon d\Omega}\right] \Big/ \frac{d^2\sigma(E, \epsilon, \theta)}{d\epsilon d\Omega}. \tag{10}$$

Here $d^2\sigma_\perp/d\epsilon d\Omega$ and $d^2\sigma_\parallel/d\epsilon d\Omega$ are respectively the bremsstrahlung cross sections for polarization perpendicular and parallel to the radiation plane given by Gluckstern and Hull (1953):

$$\begin{aligned}\frac{d^2\sigma_\perp(E, \epsilon, \theta)}{d\epsilon d\Omega} = {} & \frac{Z^2}{8\pi}\frac{r_0^2}{137}\frac{p'}{p}\frac{1}{\epsilon}\left\{\frac{-(5\gamma + 2\gamma\gamma' + 1)}{p^2\Delta^2} - \frac{(p^2 - k^2)}{Q^2\Delta^2} - \frac{2k}{p^2\Delta}\right. \\ & + \frac{L}{pp'}\left[\frac{2\gamma^2(\gamma^2 + \gamma'^2) - (5\gamma - 2\gamma\gamma' + \gamma'^2)}{p^2\Delta^2} + \frac{k(\gamma^2 + \gamma\gamma' - 2)}{p^2\Delta}\right] + \frac{l_0}{p'Q}\left[\frac{k}{\Delta} - \frac{k(p^2 - k^2}{Q^2\Delta} + 4\right] \\ & \left. - \frac{1}{p^2\sin^2\theta}\left[\frac{2L}{pp'}\left(2\gamma^2 - \gamma\gamma' - 1 - \frac{k}{\Delta}\right) - \frac{4l_0}{p'Q}(\Delta - \gamma')^2 - \frac{2l(\Delta - \gamma')}{p'}\right]\right\},\end{aligned} \tag{11}$$

$$\begin{aligned}\frac{d^2\sigma_\parallel(E, \epsilon, \theta)}{d\epsilon d\Omega} = {} & \frac{Z^2}{8\pi}\frac{r_0^2}{137}\frac{p'}{p}\frac{1}{\epsilon}\left\{\frac{8\sin^2\theta(2\gamma^2 + 1)}{p^2\Delta^4} - \frac{(5\gamma^2 + 2\gamma\gamma' + 5)}{p^2\Delta^2} - \frac{(p^2 - k^2)}{Q^2\Delta^2} + \frac{2(\gamma + \gamma')}{p^2\Delta}\right. \\ & + \frac{L}{pp'}\left[\frac{4\gamma\sin^2\theta(3k - p^2\gamma')}{p^2\Delta^4} + \frac{2\gamma^2(\gamma^2 + \gamma'^2) - (9\gamma^2 - 4\gamma\gamma' + \gamma'^2) + 2}{p^2\Delta^2} + \frac{k(\gamma^2 + \gamma\gamma')}{p^2\Delta}\right] \\ & + \frac{l_0}{p'Q}\left[\frac{4}{\Delta^2} - \frac{7k}{\Delta} - \frac{k(p^2 - k^2)}{Q^2\Delta} - 4\right] - \frac{4l}{p'\Delta} \\ & \left. + \frac{1}{p^2\sin^2\theta}\left[\frac{2L}{pp'}\left(2\gamma^2 - \gamma\gamma' - 1 - \frac{k}{\Delta}\right) - \frac{4l_0}{p'Q}(\Delta - \gamma')^2 - \frac{2l(\Delta - \gamma')}{p'}\right]\right\}.\end{aligned} \tag{12}$$

Here E is the kinetic energy of the incident electron, ϵ is the photon energy, θ is the photon angle with respect to the momentum vector of the incident electron, Z is the atomic number of the target, and $r_0 = 2.82 \times 10^{-13}$ cm. Other symbols are defined as follows:

$$\begin{aligned}& \gamma = E/mc^2 + 1; \quad \gamma' = \gamma - \epsilon/mc^2; \quad k = \epsilon/mc^2; \quad p = (\gamma^2 - 1)^{1/2}; \\ & p' = (\gamma'^2 - 1)^{1/2}; \quad L = 2\ln\left(\frac{\gamma\gamma' + pp' - 1}{k}\right); \quad l = \ln\left(\frac{\gamma + p}{\gamma - p}\right); \\ & l_0 = \ln\left(\frac{Q + p}{Q - p}\right); \quad Q^2 = p^2 + k^2 - 2pk\cos\theta; \quad \Delta = \gamma - p\cos\theta.\end{aligned} \tag{13}$$

The minus sign in front of the term $4l_0/p'Q$ in the last line of equation (11) was misprinted as a multiplication sign in Gluckstern and Hull (1953) (Gluckstern 1977, private communication).

The bremsstrahlung produced by the electrons with a distribution function of the momentum vectors,

$$g(\theta, \phi) \equiv g(\theta), \tag{14}$$

is given by

$$Q(\epsilon, \theta) = n \int_{\epsilon}^{\infty} dE \int_{-1}^{+1} d(\cos \theta_0) \int_0^{2\pi} d\phi_0 g(\theta_0) \frac{d^2\sigma(E, \epsilon, \theta')}{d\epsilon d\Omega'} N(E)v(E) . \quad (15)$$

Here $N(E)$ is the instantaneous differential electron number, n is the ambient density, $v(E)$ is the electron velocity, θ is the angle between the line of sight and the normal to the photosphere, (θ_0, ϕ_0) is the polar coordinate of the momentum vector of the electron in the system whose Z-axis is the normal to the photosphere, θ' is the angle between the line of sight and the momentum vector of the electron, and is given by

$$\cos \theta' = \cos \theta \cos \theta_0 + \sin \theta \sin \theta_0 \cos \phi_0 , \quad (16)$$

and

$$\frac{d^2\sigma}{d\epsilon d\Omega'}(E, \epsilon, \theta') = \frac{d^2\sigma_{\parallel}}{d\epsilon d\Omega'}(E, \epsilon, \theta') + \frac{d^2\sigma_{\perp}}{d\epsilon d\Omega'}(E, \epsilon, \theta') .$$

To calculate the Stokes parameters $(1, P_1, P_2)$ due to such an electron distribution, we need to find the Stokes parameters with respect to the normal plane of the bremsstrahlung by an electron beam at a given direction and integrate over the electron direction. It can be shown that one of the Stokes parameters with respect to the normal plane is given by (e.g., Haug 1972)

$$P_1(\epsilon, \theta) = \frac{1}{Q(\epsilon, \theta)} \left\{ \int_{\epsilon}^{\infty} dE \int_{-1}^{+1} d(\cos \theta_0) \int_0^{2\pi} d\phi_0 g(\theta_0) \cos 2\alpha \left[\frac{d^2\sigma_{\perp}(E, \epsilon, \theta)}{d\epsilon d\Omega} - \frac{d^2\sigma_{\parallel}(E, \epsilon, \theta)}{d\epsilon d\Omega} \right] N(E)v(E) \right\} , \quad (17)$$

where $Q(\epsilon, \theta)$ is given by equation (15), θ' is given by equation (16), and α is the angle between the radiation plane and the normal plane, which is given by

$$\cos \alpha = (\cos \theta \sin \theta_0 \cos \phi_0 - \sin \theta \cos \theta_0)/\sin \theta' . \quad (18)$$

Another Stokes parameter, $P_2(\epsilon, \theta)$, is equal to zero because of the symmetry around the normal plane.

c) *A Monte Carlo Simulation*

We evaluate the backscattering of primary photons by using a Monte Carlo simulation. Since we use the Stokes parameters which characterize an ensemble of photons, the unit of the photon flux is not an individual photon but a photon ensemble characterized by the Stokes parameters. In determining whether the absorption or Compton scattering takes place, we treat this photon ensemble as if it were an individual photon. Such a treatment increases the accuracy of the calculated polarization.

For linearly polarized photon beams, we can use an individual photon approach, by regarding the photon beam to consist of an unpolarized beam and a completely polarized beam, by choosing the polarization vector of each individual photon accordingly and by using the cross section given by equation (1) (Langer and Petrosian 1977). However, this approach is less advantageous than the approach using the Stokes parameters. In the latter approach, for a given photon beam the degree of polarization of the photons scattered along a given direction is exactly determined by the ensemble average given by equations (23) and (24). On the other hand, the degree of polarization calculated by the former approach is determined statistically and consequently contains a statistical error.

We choose the incident direction of the photon in accordance with the angular distribution of a source function $Q(\epsilon_0, \theta_0, \phi_0)$, where θ_0 and ϕ_0 are the polar and azimuthal angles of the photon in a system whose Z-axis is perpendicular to the photosphere. Photons with $\theta_0 < 90°$ move away from the Sun. We choose the initial energy of the photon, ϵ_0, such that photons are uniformly distributed in log ϵ_0 space, and we then take into account the energy spectrum of the primary X-rays by assigning each photon a weighted number proportional to its energy and the differential photon intensity at this energy. This procedure is more advantageous for two reasons than the direct generation of photons with a desired energy spectrum. First, in the latter procedure the photon count statistics decreases rapidly with increasing energy, whereas with the present method the photon count statistics remains similar in each logarithmically spaced energy bin. Second, with the present method we can get the results corresponding to initial photons with various energy spectra with only one computer run by simply assigning the appropriate weighting factors to each photon for various spectra.

Upon choosing the energy and the incident direction of the initial photon, the Stokes parameters of the photon ensemble are determined: For isotropic sources $P_1 = P_2 = 0$, and for anisotropic sources, they are given by the result calculated by using equation (17).

The Compton scattering takes place at a columnar depth of about 10^{24} cm^{-2}, where the density is about 10^{17} cm^{-3} (e.g., Gingerich *et al.* 1971) and the mean free path of the photon is of the order of 10^7 cm. Because this depth is much larger than the chromospheric and photospheric irregularities, and because the height of the X-ray source is much smaller than one solar radius, throughout this paper we assume that the photosphere is plane-stratified.

Since multiple scattering occurs, other than the initial incident direction and the initial photon energy, we need

several parameters to characterize the photon: the present direction of propagation, the present energy, the present Stokes parameters, and the vertical depth at which the previous scattering took place. Since the position of the photon interaction is expressed by the columnar depth, our calculation is independent of the solar atmospheric model, as far as the plane-stratified photosphere is assumed.

We choose the path length for the Compton scattering (in units of the hydrogen number per cm^2), X_s, and the path length for absorption, X_a, according to the cross sections given by equations (8) and (9), respectively. If $X_a < X_s$, the photon is absorbed. If $X_a > X_s$, the photon makes a Compton scattering. The scattering angles (θ_s, ϕ_s) are chosen according to equation (6). The direction of the photon after the scattering is given by (θ_2, ϕ_2), where

$$\cos\theta_2 = \cos\theta_1\cos\theta_s - \sin\theta_1\sin\theta_s\cos\phi_s\,, \tag{19}$$

$$\cos\phi_2 = (\cos\theta_1\cos\phi_1\sin\theta_s\cos\phi_s - \sin\phi_1\sin\theta_s\sin\phi_s + \sin\theta_1\cos\phi_1\cos\theta_s)/\sin\theta_2\,, \tag{20}$$

$$\sin\phi_2 = (\cos\theta_1\sin\phi_1\sin\theta_s\cos\phi_s + \cos\phi_1\sin\theta_s\sin\phi_s + \sin\theta_1\sin\phi_1\cos\theta_s)/\sin\theta_2\,. \tag{21}$$

Here (θ_1, ϕ_1) are the direction of the photon before the collision. The energy of the photon after the scattering is given by equation (2). The vertical columnar depth at which the next interaction takes place is

$$X' = X - X_t\cos\theta_2\,, \tag{22}$$

where X is the vertical depth of the present scattering point, X_t is the interaction path length, and $\cos\theta_2$ is given by equation (19). If X' becomes a negative quantity for both absorption and Compton scattering, this means that the photon escapes from the photosphere.

The relationship between the Stokes parameters with respect to the normal plane of the initial photon beam and those of the scattered beam can be found by applying appropriate rotation matrices and equation (6). If a photon beam with the Stokes parameters $(1, P_1, P_2)$ with respect to the normal plane is Compton scattered, the Stokes parameters of the scattered photon beam are given by (Bai 1977)

$$\begin{aligned} P_1' = [&\cos 2\alpha\{\sin^2\theta_s + (1+\cos^2\theta_s)(P_1\cos 2\phi_s + P_2\sin 2\phi_s)\} \\ &+ \sin 2\alpha\{2\cos\theta_s(P_2\cos 2\phi_s - P_1\sin 2\phi_s)\}]/A(\epsilon_0, \theta_s, \phi_s)\,, \end{aligned} \tag{23}$$

$$\begin{aligned} P_2' = [&\cos 2\alpha\{2\cos\theta_s(P_2\cos 2\phi_s - P_1\sin 2\phi_s)\} \\ &- \sin 2\alpha\{\sin^2\theta_s + (1+\cos^2\theta_s)(P_1\cos 2\phi_s + P_2\sin 2\phi_s)\}]/A(\epsilon_0, \theta_s, \phi_s)\,, \end{aligned} \tag{24}$$

where

$$A(\epsilon_0, \theta_s, \phi_s) = \frac{\epsilon}{\epsilon_0} + \frac{\epsilon_0}{\epsilon} - \sin^2\theta_s + \sin^2\theta_s(P_1\cos 2\phi_s + P_2\sin 2\phi_s)\,, \tag{25}$$

$$\cos\alpha = -(\cos\theta_1\sin\theta_s + \sin\theta_1\cos\theta_s\cos\phi_s)/\sin\theta_2\,, \tag{26}$$

$$\sin\alpha = \sin\theta_1\sin\phi_s/\sin\theta_2\,. \tag{27}$$

Here ϕ_s is the azimuthal angle of the scattering measured relative to the initial normal plane, and θ_2 is given by equation (19).

We follow all the photons until they escape or are absorbed. Then, we collect the reflected photons according to their final energies, ϵ, and the directions of motion, (θ, ϕ), thereby defining a source function $Q'(\epsilon, \theta, \phi)$. The energy bins are logarithmically divided from 10 keV to 500 keV, and the angular bins are 10 equally divided solid angle intervals. We generate enough photons so that in most of the bins the number of photons in one bin is larger than 100. In most cases except where the reflectivity is very small (such as $\theta \approx 90°$, or very low energy bins or very high energy bins), the number of photons is several hundred. Therefore, one standard deviation error of the Poissonian statistics is about a few percent. We further reduce the magnitudes of the errors by fitting the calculated results with smooth curves both in energy space and in angular space.

III. BACKSCATTER, ANISOTROPY, AND SPECTRAL CHARACTERISTICS OF SOLAR HARD X-RAYS

a) The Albedo of Isotropic Sources

For the calculations of this section, we use isotropic and unpolarized primary photon sources. We consider power-law sources given by

$$Q(\epsilon) = A\epsilon^{-s} \quad \text{photons sr}^{-1}\,\text{s}^{-1}\,\text{keV}^{-1}\,, \tag{28}$$

and optically thin thermal sources given by (e.g., Holt 1974)

$$Q(\epsilon) = 2.41 \times 10^{-16} g(T, \epsilon) Z^2 n_e n_i V (kT)^{-3/2} (\epsilon/kT)^{-1} \exp(-\epsilon/kT) \quad \text{photons sr}^{-1}\,\text{s}^{-1}\,\text{keV}^{-1}\,, \tag{29}$$

where ϵ and kT are in keV, Z is the atomic number of the medium, n_e and n_i are the electron and ion densities, V is the volume of the emitting source, and $g(T, \epsilon)$ is the Gaunt factor (Karzas and Latter 1961).

The observed photon spectrum consists of the sum of the initial photons and the reflected photons: $Q_T(\epsilon, \theta, \phi) = Q(\epsilon, \theta, \phi) + Q'(\epsilon, \theta, \phi)$, where $Q'(\epsilon, \theta, \phi)$ is the reflected photon spectrum. Notice here that the initial energies of the reflected photons observed at the energy ϵ must be larger than ϵ. We define the differential reflectivity for an isotropic source as

$$R(\epsilon, \theta, \phi) = Q'(\epsilon, \theta, \phi)/Q(\epsilon)\,. \tag{30}$$

With this definition, the observed photon spectrum is expressed as $Q_T(\epsilon, \theta, \phi) = [1 + R(\epsilon, \theta, \phi)]Q(\epsilon)$. The integral reflectivity is given by

$$\bar{R}(\epsilon) = (2\pi)^{-1} \int_0^{2\pi} d\varphi \int_0^1 d(\cos\theta) R(\epsilon, \theta, \varphi)\,. \tag{31}$$

Figure 1 shows the integral reflectivities of isotropic sources with power-law and thermal spectra. As can be seen, the reflectivity is maximum around 30 keV. The integral reflectivity is determined by three effects. The first is absorption due to the photoelectric effect. At lower energies the reflectivity is reduced mainly because of absorption; however, even at $\epsilon_0 = 100$ keV, one-third of the incident photons are absorbed, as was mentioned earlier. The second is energy degradation. At higher energies the reflectivity decreases mainly because of this effect, and because of this fact the reflectivity at higher energies is larger for flatter spectra. The third effect is the compression in energy space which is caused by the fact that the energy degradation becomes larger with the increase of energy. This effect makes the reflectivity larger, and because of this effect the integral reflectivity at 30 keV for $s = 2$ is larger than 0.5 even though only 50% of the photons incident with $\epsilon_0 = 30$ keV escape from the photosphere.

Figure 2 shows the differential reflectivity for three values of θ and three incident photon spectra. (Here θ is the polar angle of the reflected photon in the point of view of the source, and is the heliocentric angle of the source in the point of view of the observer.) As can be seen, below $\sim$250 keV the reflectivity is larger at smaller values of θ, because the amount of matter traversed is smaller in these cases. The trend is reversed at higher energies, because at these energies the cross section for large angle scattering is small.

The idea that solar hard X-rays are produced by hot thermal electrons began to gather new interest recently (Colgate, Audouze, and Fowler 1977). In Figure 3 we show the total (primary and reflected) photon spectrum of

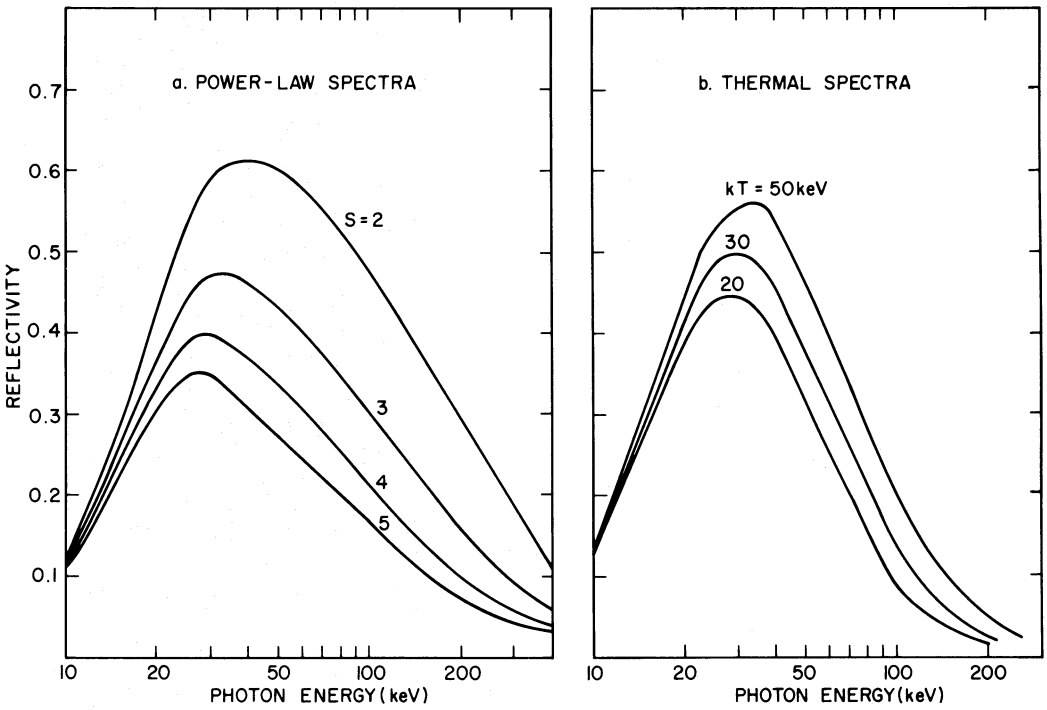

FIG. 1.—Integral reflectivities of isotropic X-ray sources. The reflectivity is defined in eqs. (30) and (31).

thermal X-ray sources for $kT = 20$ and 30 keV and two directions of observation. As can be seen, even though the total spectra are somewhat steeper than the primary spectra, they still resemble thermal spectra.

b) Anisotropic Sources

For the anisotropic sources, we assume that X-rays are produced by accelerated electrons with momentum vectors uniformly distributed in a cone of 30° half opening angle centered around the downward vertical vector. The distribution function of the momentum vectors of such electrons is

$$g(\theta') = 1/[2\pi(1 - \cos 30°)] \quad \text{for } 150° \leq \theta' \leq 180°$$
$$= 0 \quad \text{otherwise}, \tag{32}$$

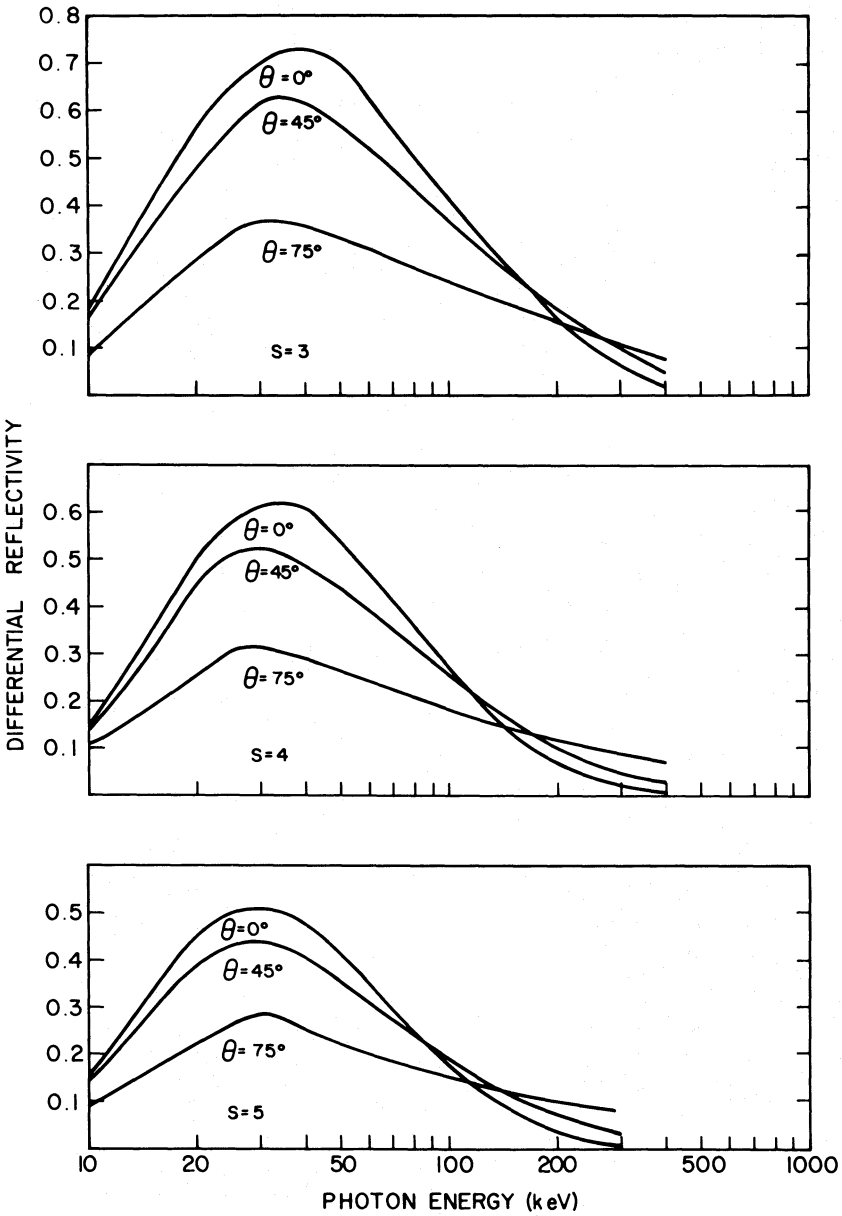

FIG. 2.—Differential reflectivities of isotropic sources with power-law spectra

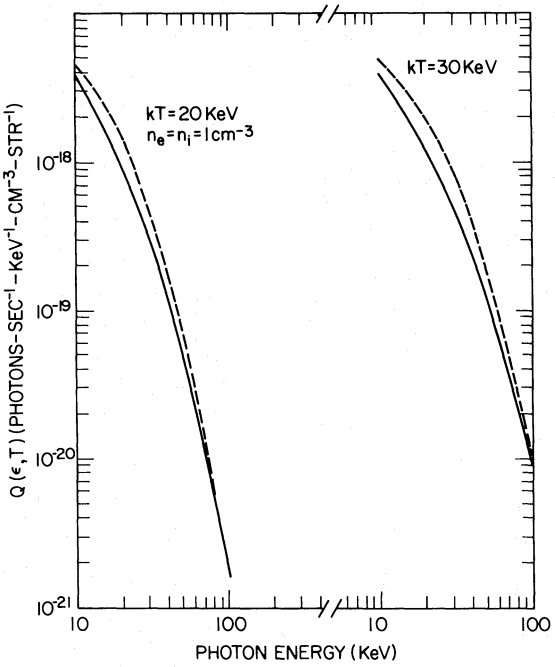

FIG. 3.—Photon spectra due to a thermal hydrogen plasma with $n_e = n_i = 1$ cm^{-3}, and $kT = 20$ keV and $kT = 30$ keV. The resultant spectra (including the reflected component) seen at $\theta = 0°$ are shown by the dashed lines. The solid lines indicate the original spectrum.

where θ' is the polar angle measured from the normal to the plane-stratified photosphere. Though a unidirectional beam of electrons is easier to deal with, we introduce the finite dispersion of the velocity vectors of the electrons for the following reasons: (1) The electrons will have finite pitch angles. (2) The magnetic field lines guiding the electrons are not expected to be exactly straight or vertical. (3) As discussed by Brown (1972), collisions of the electrons with ambient particles cause the dispersion of the pitch angles. We also assume that the instantaneous electron energy spectra are power laws with power indices 2.5 and 3.5.

Using equations (15), (11), (12), and (32), and using $N(E) \sim E^{-2.5}$ for the electron spectrum, we calculate the X-ray production rate, $Q(\epsilon, \theta)$, for various values of ϵ and θ. Similarly we also calculate the degree of polarization, $P_1(\epsilon, \theta)$, by using equations (17), (11), and (12). The degree of polarization is plotted in Figure 4, and the X-ray production rates are shown by solid lines in Figure 5. In this figure, 90° corresponds to X-ray emission from the solar limb and 0° to emission from the disk center. Without the reflection of the X-rays, there would be a large limb brightening and a slight limb flattening of the photon spectra. Similar results were obtained by Brown (1972) and by Petrosian (1973).

Using the Monte Carlo simulation described in the preceding section, we calculate the backscatter of the photons whose polarization and spectrum and angular distribution are shown in Figures 4 and 5, respectively. The dashed lines in Figure 5 show the resultant total photon production rates including the primary and reflected sources. Similar calculations were performed for the electron spectrum $N(E) \sim E^{-3.5}$. The results are shown in Figures 6 and 7, in a manner similar to Figures 4 and 5.

As can be seen in Figures 4 and 6, for the anisotropic model we use, the degree of polarization of the primary X-rays is very large, especially at low photon energies and near 90°. The degree of polarization of the hard X-rays observed near the Earth, however, will be modified by the dominant backscattered component. The degree of polarization including the backscattered component will be studied in the next section.

As can be seen in Figures 5 and 7, the limb brightening effect has almost disappeared, except at very low energies or at very high energies where the reflectivity is small (Fig. 1). Henoux (1975) has also reported similar results. Therefore, the anisotropic model in which electrons are moving toward the photosphere is not contradictory to the observational results of Datlowe *et al.* (1974, 1977) when the reflected component is properly taken into account. Therefore, the lack of limb brightening effect does not rule out the possibility that the accelerated electrons move predominantly down toward the photosphere; this interpretation is contradictory to that of Datlowe *et al.* (1974, 1977).

Figure 8 shows the photon spectra due to anisotropic sources, taken from Figures 5 and 7 for several observation angles. Even though over the entire energy range the photon spectra deviate from power laws, in the 15–50 keV range they can be reasonably well approximated by a single power law. Similar approximations can be made for the isotropic power-law sources. The resultant spectral indices for this energy range are shown in Table 1. As can

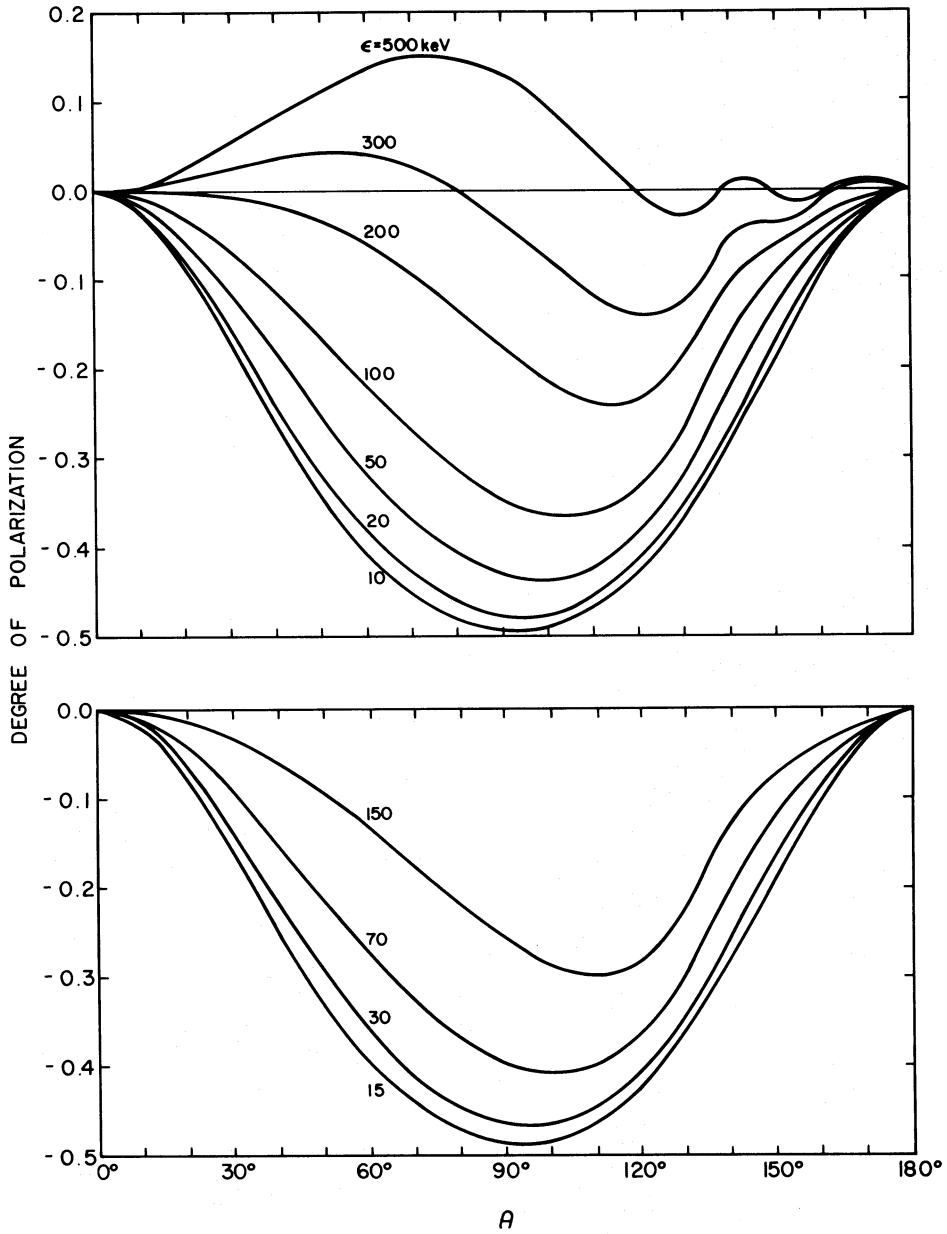

FIG. 4.—The degree of polarization of primary hard X-rays due to the accelerated electrons moving toward the photosphere with velocity vectors uniformly distributed in a cone with half opening angle 30° and centered at the vertical to the photosphere. The spectrum of the accelerated electrons is $E^{-2.5}$. The negative values mean that the direction of polarization is parallel to the normal plane; the positive, perpendicular.

be seen, for the isotropic sources, the spectral index does not change appreciably with heliocentric angle because reflection is not the dominant source of photons in this case. On the other hand, for the anisotropic sources the photon spectrum steepens as the heliocentric angle increases, a fact that can account for the result of Datlowe, Elcan, and Hudson (1974) who found that the average spectral index (in the 17 to 45 keV range) of limb flares is larger by about 0.5 than that of disk flares.

Another characteristic of the spectra shown in Figure 8 is that for flares near the disk center the spectra steepen as energy increases, but this character is less pronounced for limb flares (see Table 2). Therefore, if the accelerated electrons in flares move predominantly downward, the spectra measured at energies $\gtrsim 100$ keV will show a limb flattening in contrast to the spectra measured at energies $\lesssim 50$ keV. This may be tested in future experiments. If the steepening of the spectrum at energies $\gtrsim 100$ keV is larger for flares near the disk center than for flares near the limb, it can be regarded as a supporting evidence for the anisotropic model. The spectral characteristics up to

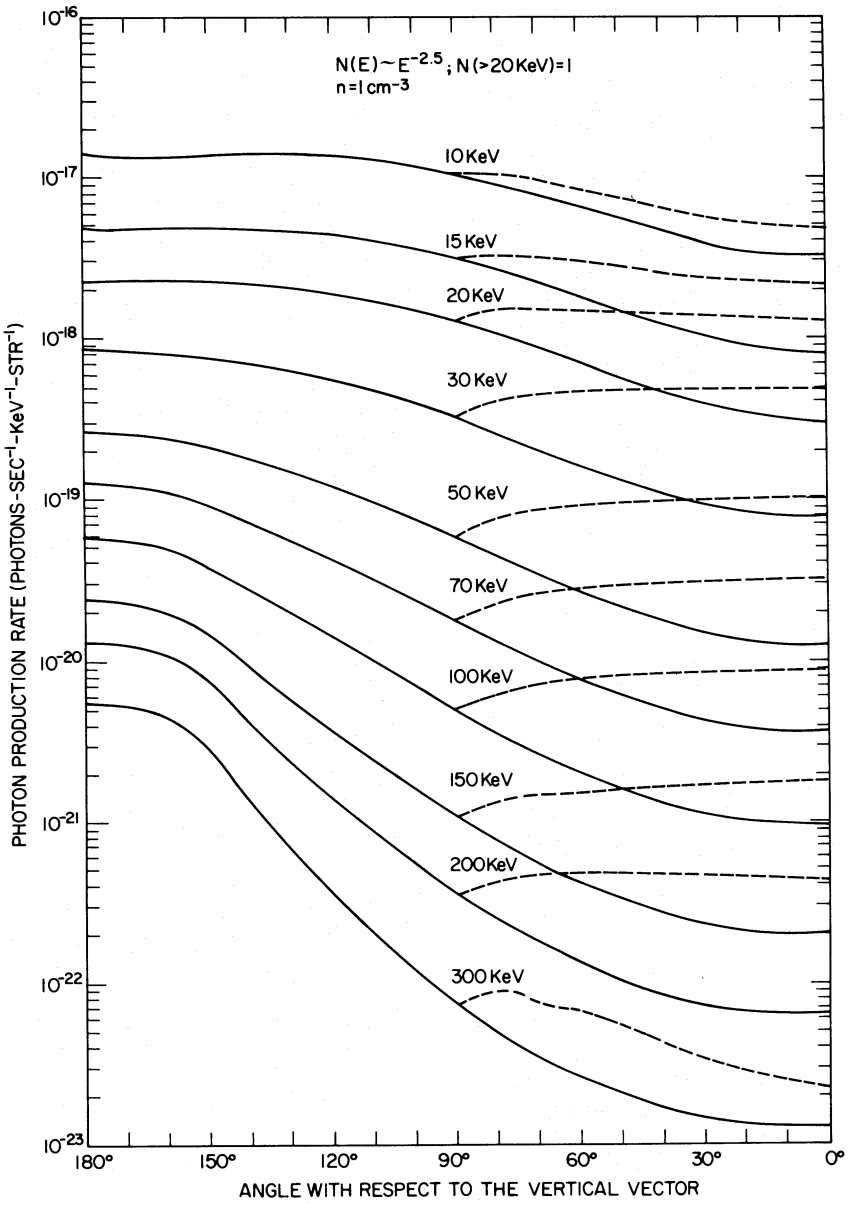

FIG. 5.—X-ray intensities due to the same electrons as in Fig. 4. The solid lines represent primary photon intensities and the dashed lines represent the sum of the primary and reflected photons.

300 keV will be available from the measurements of the hard X-ray spectrometer (Frost 1976) which will be included in the payload of NASA's Solar Maximum Mission.

IV. COMPTON BACKSCATTER AND POLARIZATION

As we have seen in § III, for the anisotropic model in which accelerated electrons move downward, the backscattered component dominates the observed flux except for flares very close to the limb. For an isotropic source, the backscattered component constitutes a small fraction of the observed flux. However, the backscattered photons are polarized due to the polarization dependence of the Compton scattering cross section. Therefore, in calculating the polarization of solar hard X-rays, we have to take into account the effect of the backscatter on the polarization. In calculations of the polarization until now, however, the effect of Compton backscatter was not considered except by Henoux (1975) and by Langer and Petrosian (1977).

Even though in the calculations of the preceding section the polarization of the photon was followed throughout the scattering process, the polarization of the backscattered photons was not recorded. To calculate the degree of

TABLE 1

SPECTRAL INDICES OF PHOTON SPECTRA IN THE RANGE FROM 15 keV TO 50 keV

A. ISOTROPIC PHOTON SOURCES WITH POWER-LAW SPECTRA

ORIGINAL PHOTON SPECTRAL INDEX	θ		
	0°	45°	75°
2	1.76	1.78	1.88
3	2.84	2.87	2.94
4	3.94	3.96	3.95
5	4.99	4.97	4.93

B. ANISOTROPIC SOURCES

SPECTRAL INDEX OF THE ELECTRONS	θ					
	0°		45°		75°	
	No Reflection	Reflection	No Reflection	Reflection	No Reflection	Reflection
2.5	3.48	2.56	3.52	2.77	3.40	3.05
3.5	4.44	3.73	4.49	3.95	4.39	4.11

polarization of the backscattered photons, we need better count statistics. Using the Monte Carlo simulation described in § II, we have calculated the degree of polarization due to the Compton backscatter of isotropic monoenergetic photon sources with $\epsilon_0 = 15$ keV and $\epsilon_0 = 30$ keV, by generating 4×10^4 photon ensembles for each case. Here we use monoenergetic sources in order not to worry about the effect of energy degradation and the spectral dependence of the reflectivity. Figure 9 shows the result. Here the polarization is parallel to the normal plane. The dashed lines represent the degree of polarization of the reflected photons only, and the solid lines represent the degree of polarization of the sum of the reflected and the primary photons. The dotted line shows the degree of polarization of the single-scattered photons only, which can be calculated analytically. This result is consistent with the result of the Monte Carlo simulation.

As can be seen in this figure, the degree of polarization of the sum of the reflected and the primary unpolarized photons is less than 4%. This result is consistent with the result by Henoux (1975) and Beigman (1973). In contradiction to the above result, Brown, McClymont, and McLean (1974) argued that the polarization due to an isotropic unpolarized primary source might be quite large because of the backscattered component; however, they did not perform an actual calculation.

Figure 10 shows the degree of polarization due to backscatter of an anisotropic primary source, whose angular distribution function and degree of polarization are given in Figures 6 and 7, respectively. Here the polarization is also parallel to the normal plane. The dashed lines show the degree of polarization of the photon flux due to the primary source only and that due to the scattered photons only. The solid lines show the degree of polarization of the sum of the primary photons and the reflected photons. For this evaluation, we use the relative contribution of the reflected photons and that of the primary photons shown in Figure 6. As can be seen, for such an anisotropic model, the degree of polarization is very large for flares far from the disk center. It is about 60% at $\theta = 90°$, and decreases monotonically to zero at $\theta = 0°$.

To see the effect of the angular dispersion of the momentum vectors of the accelerated electrons producing hard X-rays, we made a similar calculation for an anisotropic model where the electron momentum vectors are distributed uniformly in a cone with half opening angle 60° centered on the vertically downward direction. The result is shown in Figure 11. Here the degree of polarization is less than the result in Figure 10, as expected because of a larger dispersion of the momentum vectors. However, in this case also, the degree of polarization is substantial. Note that the similarities of the degree of polarization for two energies (Figs. 9–11) justify the calculation of polarization using monoenergetic sources.

TABLE 2

SPECTRAL INDICES OF PHOTON SPECTRA IN THE RANGE FROM 100 TO 300 keV FOR THE ANISOTROPIC CASES

SPECTRAL INDEX OF THE ELECTRONS	θ		
	0°	45°	75°
2.5	5.40	4.65	3.95
3.5	6.44	5.61	5.12

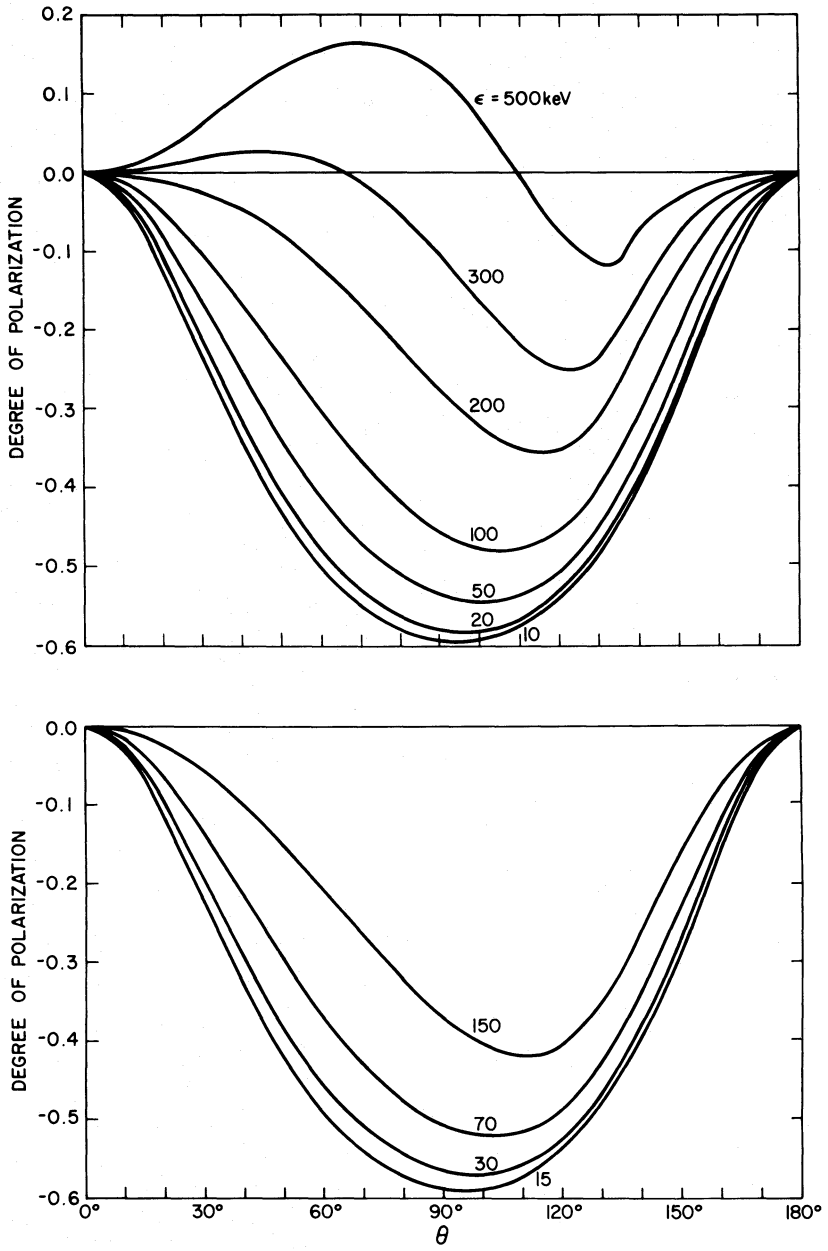

FIG. 6.—Same as Fig. 4 except that the electron spectrum is $E^{-3.5}$

V. CHARACTERISTICS OF THE ALBEDO PATCH

In this section we investigate the characteristics of the albedo patch, which is a bright X-ray patch on the photosphere created by the Compton backscatter. In this section we assume that the primary source is a point source. An extended primary source can be regarded as a superposition of many point sources, and in principle the albedo brightness distribution of an extended source can be obtained from the result for a point source.

The surface brightness of the albedo patch (measured in photons sr^{-1} cm^{-2} s^{-1}) observed at an angle θ in the energy interval from ϵ_1 to ϵ_2 is proportional to the number of photons incident upon unit area and their probability of reflection (for the geometry, see Fig. 12):

$$I(\epsilon_1 \sim \epsilon_2, \theta, l, \phi) = \bar{Q}(\epsilon_1 \sim \epsilon_2, \theta_0, \phi)\{2\pi h^2[(l/h)^2 + 1]^{3/2}\}^{-1} R(\epsilon_1 \sim \epsilon_2, \theta_0, \theta, \phi)\,. \quad (33)$$

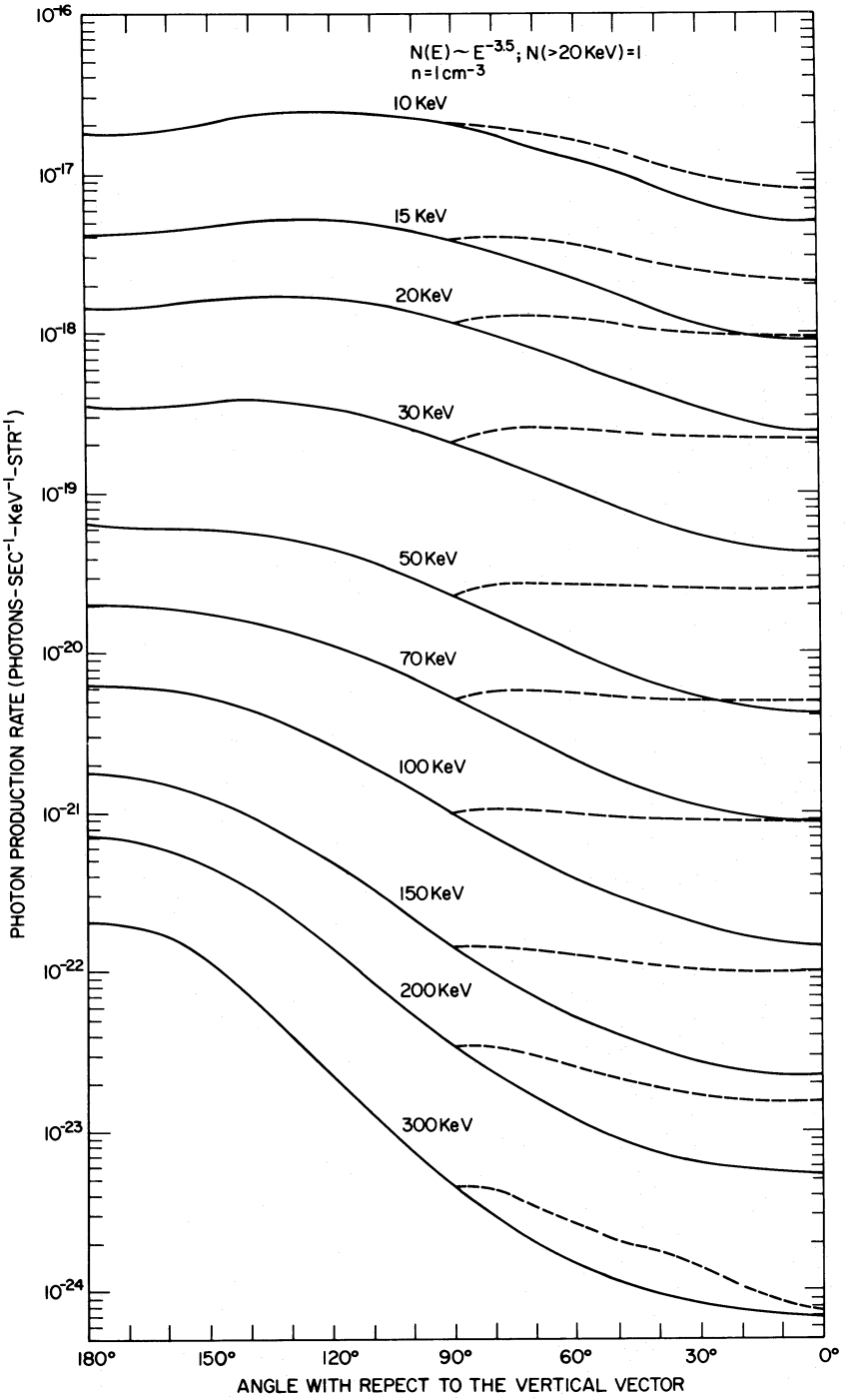

FIG. 7.—Same as Fig. 5 except that the electron spectrum is $E^{-3.5}$

Here the first factor, $\bar{Q}(\epsilon_1 \sim \epsilon_2, \theta_0, \phi)$, represents the angular distribution of the incident photons in the energy interval $\epsilon_1 \sim \epsilon_2$; the second factor relates a unit solid angle to the area on the photosphere where h is the height of the source and $l = -h \tan \theta_0$; and $R(\epsilon_1 \sim \epsilon_2, \theta_0, \theta, \phi)$ is the differential reflectivity of a beam of photons. It is defined as

$$R(\epsilon_1 \sim \epsilon_2, \theta_0, \theta, \phi) = \frac{2\pi \int_{\epsilon_1}^{\epsilon_2} d\epsilon Q'(\epsilon, \theta, \phi)}{\int_{\epsilon_1}^{\epsilon_2} d\epsilon Q_{\theta_0}(\epsilon)}, \tag{34}$$

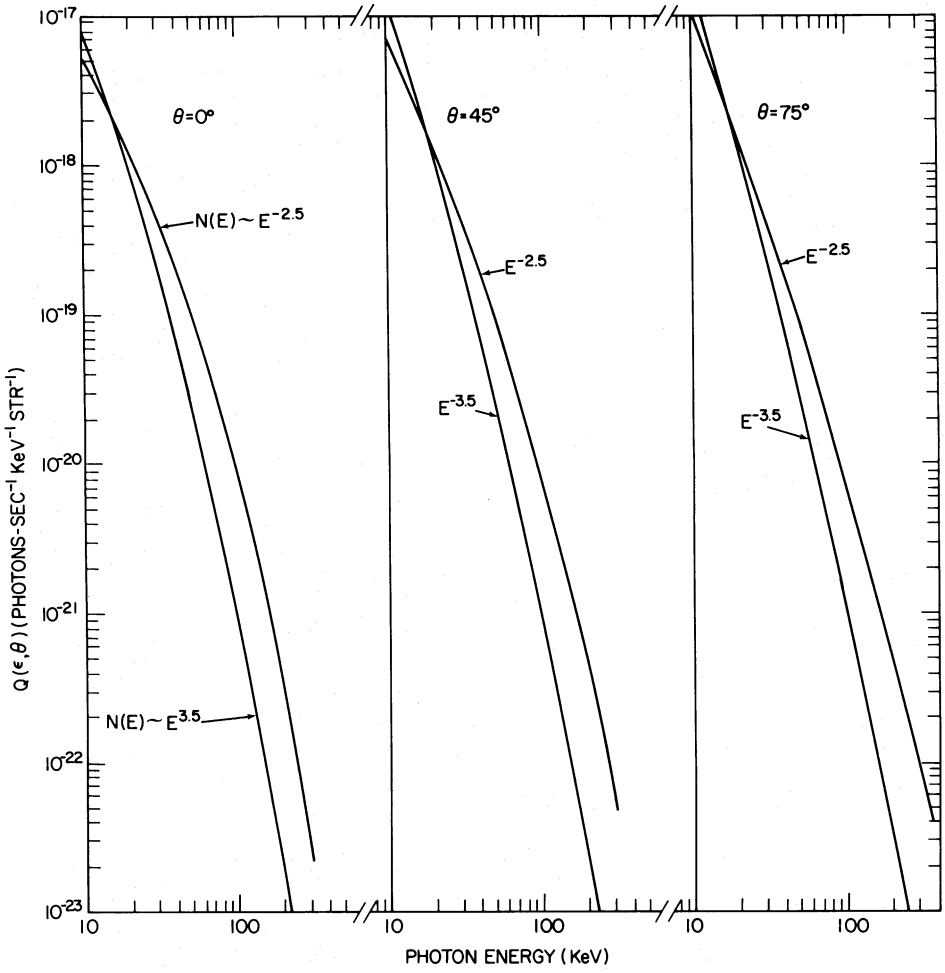

FIG. 8.—Photon spectra taken from the results of Figs. 5 and 7; θ is the angle between the direction of observation and the normal to the photosphere.

where $Q_{\theta_0}(\epsilon)$ represents a beam of primary photons incident at θ_0, and $Q'(\epsilon, \theta, \phi)$ is the photon source due to reflection. Equation (33) implicitly assumes that the photon enters and escapes from the photosphere at the same position. This assumption is generally valid because the height of the X-ray source is believed to be much larger than the mean free path of the photon in the photosphere, which is only about 10^7 cm (§ IIc).

Through the second factor in equation (33), h affects the brightness distribution of the albedo patch. Thus, by measuring the albedo brightness distribution, we might be able to deduce h. This was first pointed out by Brown, van Beek, and McClymont (1975); however, in their calculation it was assumed that the reflection probability was constant. As will be shown, because it depends on the directions of the incident and outgoing photons and also on the polarization, this fact should be taken into account for a better deduction of h.

The value of the differential reflectivity, $R(\epsilon_1 \sim \epsilon_2, \theta, l, \phi)$, is determined by the combined effects of the angular dependence of the Compton scattering cross section and the probability for escape determined by the amount of material traversed before and after the scattering process. For example, for a given observation angle θ, R increases as θ_0 decreases from vertical incidence ($\theta_0 = 180°$), mainly because less material is traversed by the escaping photons when θ_0 is small than when θ_0 is large. For a given θ_0 ($>90°$), R decreases as θ increases from $\theta = 0°$ (vertical escape) because also in this case increasingly larger amounts of material are traversed by escaping photons. Another angle-dependent factor of R is due to the Compton cross section. Mainly because of this factor, R depends on ϕ. And through this factor, the state of polarization of the primary source strongly affects the albedo brightness distribution.

Because the X-ray emission of the anisotropic primary source considered in this paper is partially polarized along the normal plane, such X-ray emission can be regarded as consisting of an unpolarized emission and a completely plane-polarized emission. Thus, it would be convenient to have calculations of the differential reflectivity of a completely unpolarized beam of photons and also of a completely plane-polarized beam of photons, for various

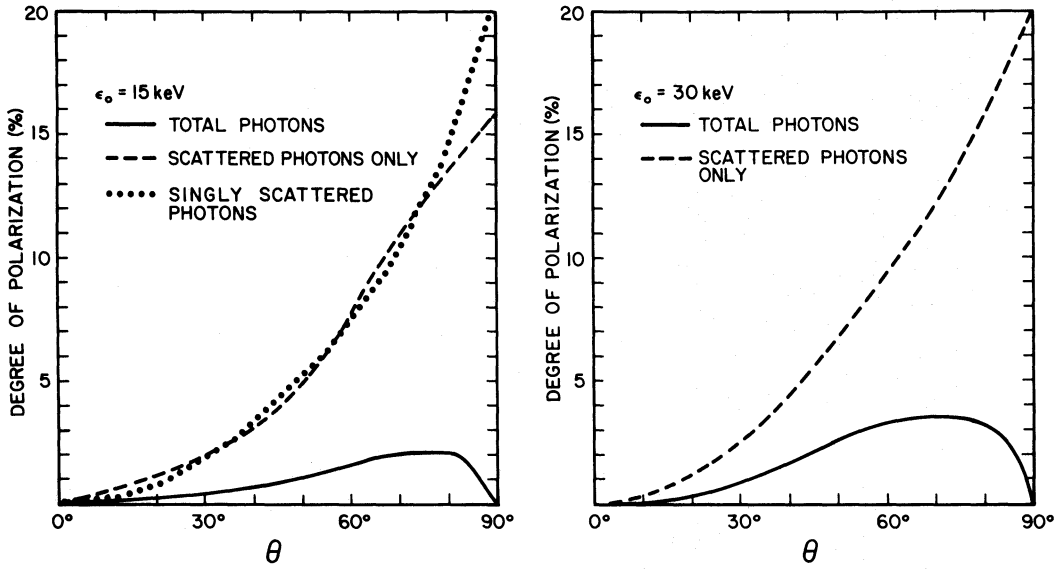

FIG. 9.—Degree of polarization due to Compton backscatter of unpolarized isotropic primary photons. The dashed lines represent the degree of polarization of the scattered photons only, and the solid lines represent the degree of polarization of the sum of the primary and reflected photons. The dotted line represents the degree of polarization of singly scattered photons alone. The direction of polarization is along the normal plane.

beam directions. From such results the differential reflectivity of a beam of photons with an arbitrary degree of polarization can be obtained.

Considering the steep energy spectra of solar hard X-rays and the energy dependence of the reflectivity, we find that the second highest energy bin of the Hard X-ray Imaging Spectrometer, from 16 to 22 keV, is most suitable for albedo measurements. Therefore, we calculate the differential reflectivity in this energy interval, for various beam directions ($\theta_0 = 180°, 170°, 160°, \ldots, 100°$) and for the two states of polarization. We calculate for three power-law spectra of the incident beams (ϵ^{-3}, ϵ^{-4}, and ϵ^{-5}), and we fit the results for the spectrum ϵ^{-3} with smooth curves in Figures 13 and 14. (The results for the other spectra show similar properties as in these figures.)

The major characteristics of the differential reflectivity of an unpolarized beam as a function of the beam

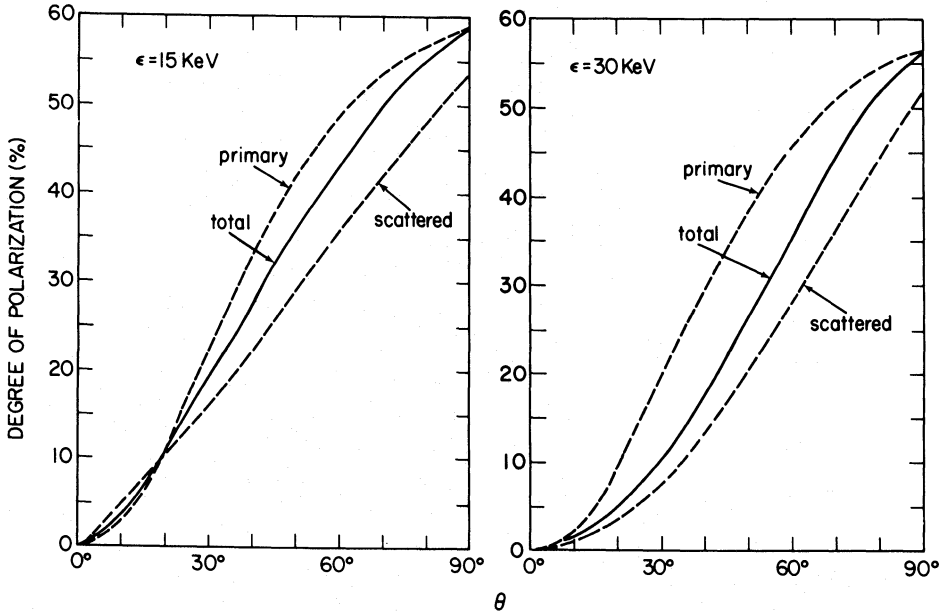

FIG. 10.—Degree of polarization of photons due to anisotropic electrons, where the angular distribution of the electrons is

$$g(\theta) = \text{const.} \quad \text{for} \quad 150° < \theta < 180°$$
$$= 0 \quad \text{for} \quad \theta < 150°.$$

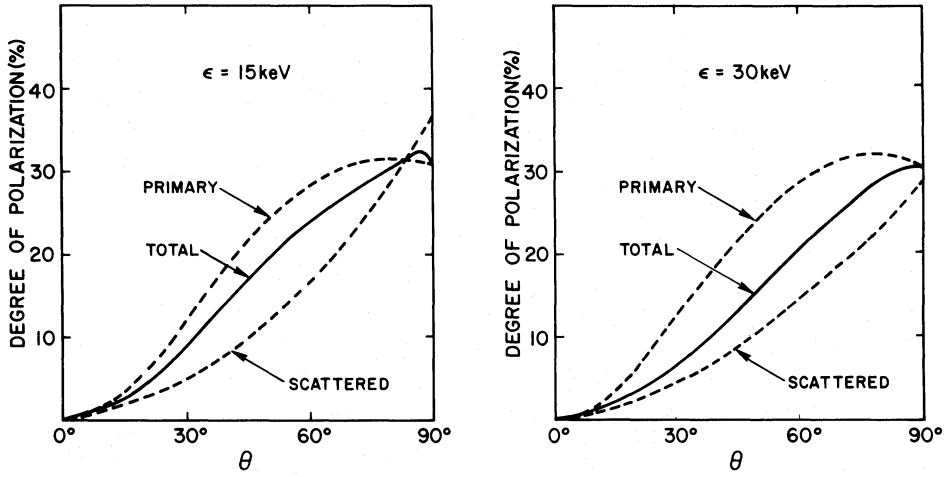

FIG. 11.—Same as Fig. 10 except that

$$g(\theta) = \text{const.} \quad \text{for} \quad 120° < \theta < 180°$$
$$= 0 \quad \text{for} \quad \theta < 120°.$$

direction are easily noticed from Figure 13. They are summarized as follows: (1) for $\theta \approx 0°$ (flares at the disk center), the differential reflectivity decreases slowly as the beam direction θ_0 decreases from 180° to 90°. (2) For large values of θ (flares away from the disk center), the differential reflectivity increases as the beam direction θ_0 decreases. The net effects of these characteristics are as follows: For flares near the disk center, the scale size of the albedo patch will be smaller than that obtained by assuming that the reflectivity is independent of the incident direction; on the other hand, for flares away from the disk center ($\theta \gtrsim 35°$), the scale size of the albedo patch will be larger.

The differential reflectivity of a completely polarized beam of photons (the Stokes parameters with respect to the normal plane are $P_1 = -1$, $P_2 = 0$) are shown in Figure 14. From the comparison of Figures 14 and 13, the differences are self-evident. These differences are due to the fact that, for the Stokes parameters $P_1 = -1, P_2 = 0$, the scattering cross section is largest at $\phi = 90°$ or 270° and is smallest at $\phi = 0°$ or 180°, at a given scattering angle θ_s (see eq. [6]). The reason why the reflection probability at $\phi = 180°$ is generally much larger than at $\phi = 0°$ is as follows. From the geometry of the problem, for given θ and θ_0, $\sin \theta_s$ is smaller when $\phi = 180°$ than when $\phi = 0°$; thus the effect of polarization on the scattering cross section is small when $\phi = 180°$.

The isobrightness contours of the albedo patch are drawn for several cases in Figure 15 with the scale in units of the height h. Starting from the center, the albedo brightness drops by a factor $\frac{1}{2}$ from one contour to the next. For the polarized source used in this figure, we assume that the photon spectrum is ϵ^{-3} regardless of the incident direction, and that the degree of polarization is the same as the degree of polarization of 20 keV photons shown in Figure 4. For the anisotropic source for this figure, we also assume that the photon flux is constant in the downward hemisphere. As can be seen, the albedo patch due to the polarized primary source near disk center is slightly smaller

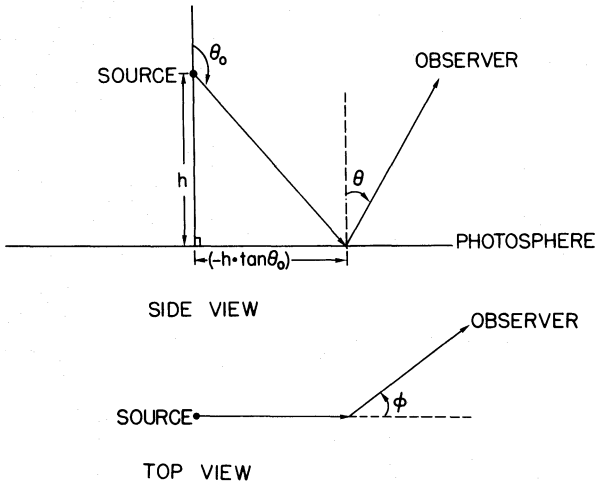

FIG. 12.—A schematic drawing of the geometry of the scattering. The angle θ is the angle of observation, and it is also the heliocentric angle of the flare in the geocentric point of view.

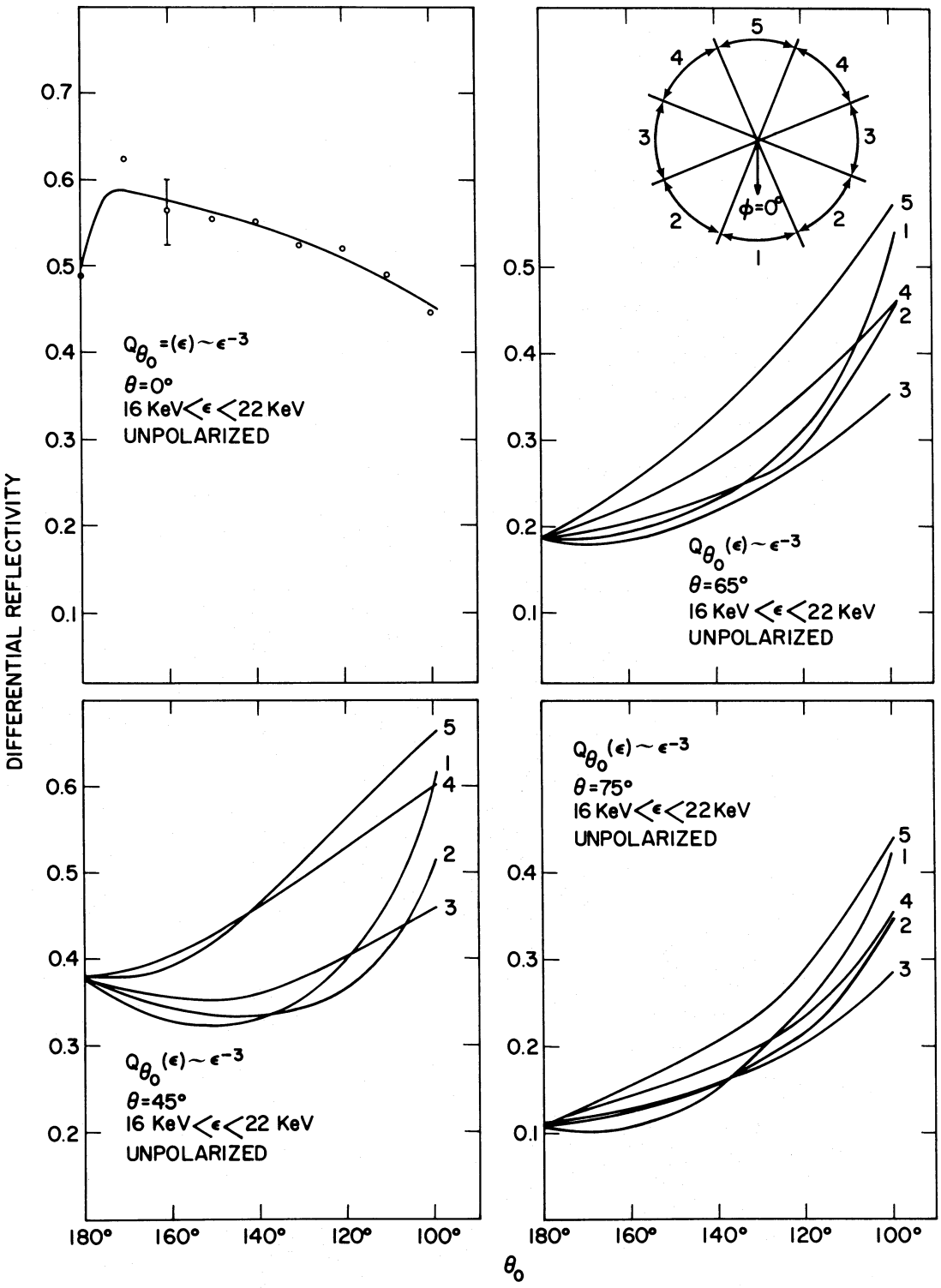

FIG. 13.—The differential reflectivity of an unpolarized beam as a function of the beam direction. It is measured in the interval from 16 to 22 keV, and the spectrum of the incident beam is ϵ^{-3}. The error bar in the upper left panel represents a typical one-sigma error, and open circles represent the result of the Monte Carlo simulation.

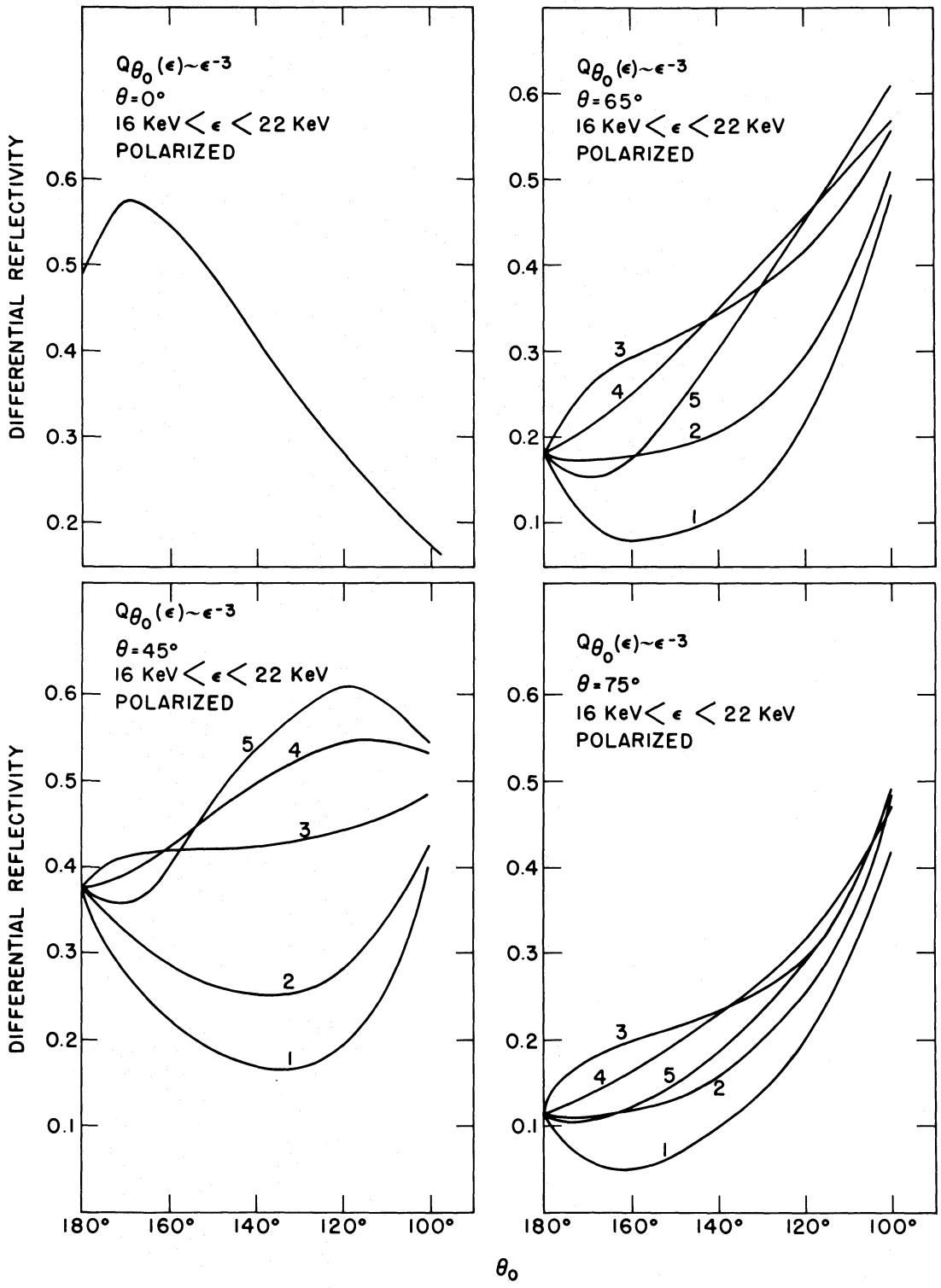

FIG. 14.—The differential reflectivity of a completely polarized beam as a function of the beam direction. The energy interval is from 16 to 22 keV, and the incident photon spectrum is ϵ^{-3}.

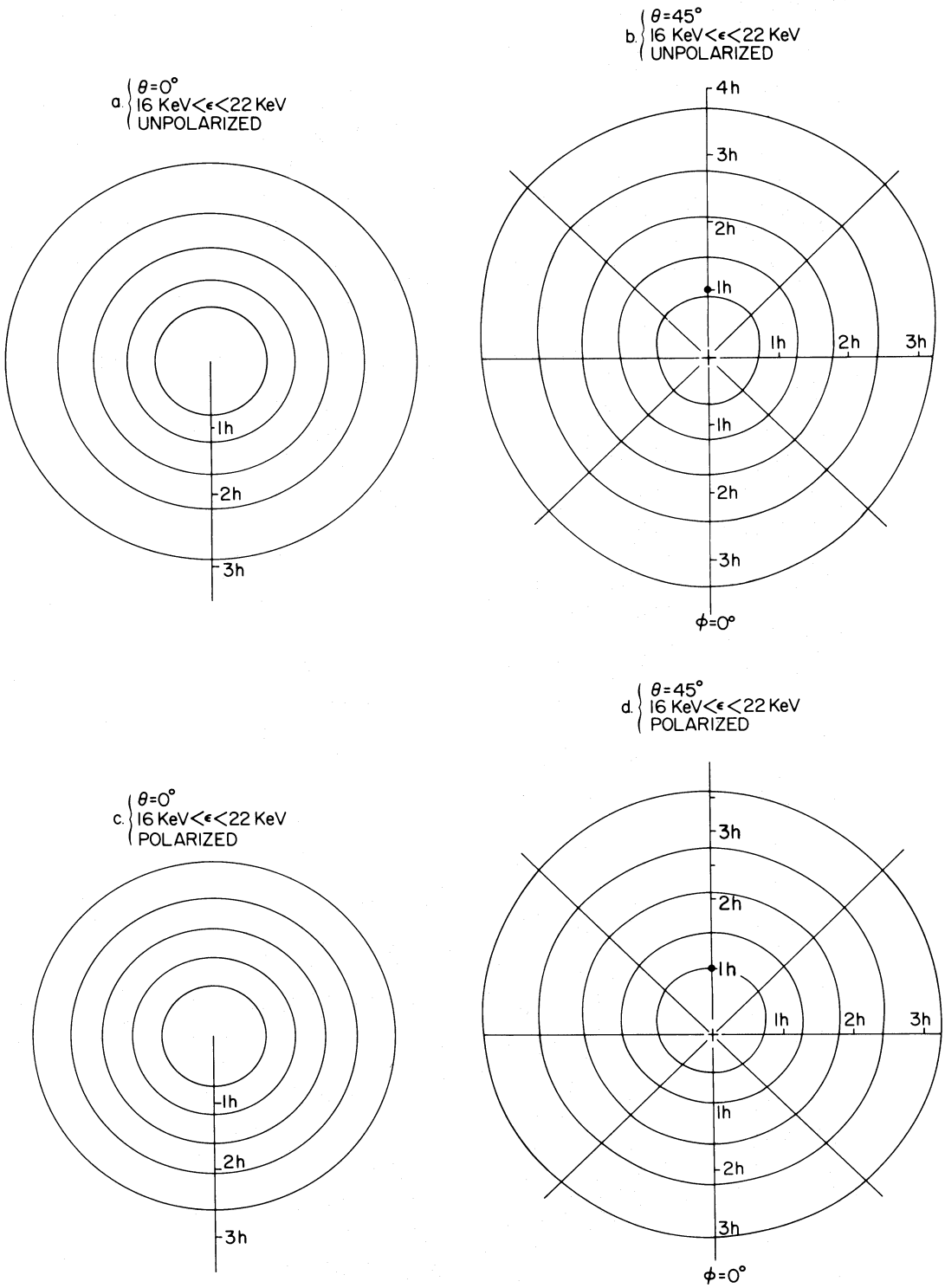

FIG. 15.—Isobrightness contours of the albedo patch for various cases. Starting from the center brightness drops by a factor $\frac{1}{2}$ from one contour to the next. See text for the explanation for polarized cases (*c* and *d*).

than that due to the unpolarized primary source with the same condition. In addition to the effect of polarization, the anisotropic distribution of the primary X-rays affects the albedo brightness distribution. However, for $\epsilon \lesssim 20$ keV the photon flux incident upon the photosphere is more or less constant independent of the incident angle (see Figs. 5 and 7). From Figure 15*d*, we notice that the albedo brightness of the polarized primary source away from the disk center is quite asymmetric about the upward-downward reflection. The surface brightness drops faster in the downward directions ($0° < \phi < 90°$ and $270° < \phi < 360°$) than in the upward directions ($90° < \phi < 270°$). For example, for $\phi = 0°$ the surface brightness at $3h$ is $\frac{1}{32}$ of that at the centroid of the patch, whereas for $\phi = 180°$ it is about $\frac{1}{20}$. Thus, from the shape of the albedo brightness contours, we may be able to learn about the state of polarization of the primary X-ray emission. However, in order to use this technique we should determine the position of the vertical projection of the primary source (the brightest point of the albedo patch) within the error of $0.1h$.

Black dots (●) in the figure represent the projection on the albedo patch of the primary X-ray source along the line of sight, and the cross marks (+) in the figure represent the centroid of the albedo patch. The distance between these two is $h \tan \theta$. Thus, the measurement of this distance can also give information on the height of the primary source.

VI. DISCUSSION AND SUMMARY

To check the correctness of our calculations, we compare our results with calculations of other researchers, wherever similar calculations are available. Agreements are generally good, and the differences can be easily attributed to the differences in the assumptions. We also compare our Monte Carlo results with the approximate analytical results, whenever they can be easily obtained with simple approximations. The results obtained by both methods are in good agreements, and the differences can be accounted for by the approximations made for the analytical calculations.

The researchers who have calculated the polarization of solar hard X-rays until now have not reported that there exists a misprint in one of the formulae for the polarization cross sections by Gluckstern and Hull (1953; Gluckstern 1977, private communication; see § II). The error in the calculations of polarization caused by overlooking this misprint is of the order of 10%. Since we use the corrected formula, our results are more accurate in this sense.

We also compare our work with the recent paper of Langer and Petrosian (1977). They assumed that the injection spectra of accelerated electrons are in the form of power laws, whereas we have assumed power laws for the instantaneous electron spectra in the interaction region. When compared after appropriate conversions, the photon spectra below about 100 keV are compatible. However, due to the energy loss of the electrons and their confinement to zero pitch angles, the steepening of the photon spectra above 100 keV is much larger in Langer and Petrosian's (1977) calculations than in ours. Furthermore, the finite angular dispersion of electron momenta assumed in our calculation leads to a smaller degree of polarization than that obtained by these authors.

Now we proceed to summarize our results.

Though a quite significant fraction of photons incident upon the photosphere with energy $\gtrsim 15$ keV are backscattered, for isotropic sources, the effect on the photon spectrum due to the backscatter is not easily observable. For anisotropic sources which emit hard X-rays predominantly toward the photosphere, the effects of the backscatter are significant. Because of the backscatter, the large limb brightening effect, which would be expected otherwise for such anisotropic sources, is canceled. For such anisotropic sources, the observed photon spectrum in the 15 to 50 keV range steepens as the flare location moves toward the limb. Such a limb steepening and the lack of limb brightening effect are compatible with the data of Datlowe, Elcan, and Hudson (1974). For such anisotropic models, the spectrum above 100 keV is steeper than the spectrum at lower energies, particularly for flares near the disk center.

In the observed photon flux, the backscattered photons are generally dominant for anisotropic sources considered in this paper. The degree of polarization of the total flux (primary flux plus reflected flux) at 15 keV or 30 keV is zero at the disk center and monotonically increases to large values at the limb. Even in the anisotropic case where the angular dispersion of electron momenta is 60°, the degree of polarization can be as large as 30%. On the other hand, for isotropic, unpolarized sources, the degree of polarization of the total flux is less than 4% even at the maximum. Thus, the measurements of polarization can be a powerful probe for the anisotropy of the accelerated electrons. The measurements by Tindo *et al.* (1970, 1972*a*, *b*, 1973), though they are somewhat tentative in nature, show quite large degrees of polarization, which cannot be attributed to the backscatter of the isotropic, unpolarized primary source. Nakada, Neupert, and Thomas (1974) also reported the measurements of finite polarization. These measurements indicate that the X-rays with energy $\gtrsim 15$ keV are very likely to be produced by anisotropic (nonthermal) electrons.

Provided that the surface brightness of the albedo patch is measured in detail, the ratio between primary and reflected photon fluxes, the size of the albedo patch, and the displacement of the primary X-ray source from the centroid of the patch, can give information on the anisotropy and the height of the X-ray source. Since we have no information on the size and shape of the primary source, we do not discuss the albedo of extended sources. But

we point out that when X-ray measurements with good spatial resolution become available, we may know the shape, size, and brightness distribution of the primary source. Then by regarding the extended primary source as a superposition of many point sources, and using the result of this work, we may be able to deduce the height of the extended source.

REFERENCES

Bai, T. 1977, Ph.D. thesis, University of Maryland (GSFC X-660-77-85).
Beigman, I. L. 1975, *Soviet Astr.—AJ*, **18**, No. 5, 600.
Brown, J. C. 1972, *Solar Phys.*, **26**, 441.
Brown, J. C., McClymont, A. N., and McLean, I. S. 1974, *Nature*, **247**, 448.
Brown, J. C., van Beek, H. F., and McClymont, A. N. 1975, *Astr. Ap.*, **41**, 395.
Colgate, S. A., Audouze, J., and Fowler, W. A. 1977, *Ap. J.*, **213**, 849.
Datlowe, D. W., Elcan, M. J., and Hudson, H. S. 1974, *Solar Phys.*, **39**, 155.
Datlowe, D. W., O'Dell, S. L., Peterson, L. E., and Elcan, M. J. 1977, *Ap. J.*, **212**, 561.
Elwert, G., and Haug, E. 1970, *Solar Phys.*, **15**, 234.
Fireman, E. L. 1974, *Ap. J.*, **187**, 57.
Frost, K. J. 1976, GSFC X-682-76-238.
Gingerich, O., Noyes, R. W., Kalkofen, W., and Cuny, Y. 1971, *Solar Phys.*, **18**, 347.
Gluckstern, R. L., and Hull, M. H. 1953, *Phys. Rev.*, **90**, 1003.
Haug, E. 1972, *Solar Phys.*, **25**, 425.
Henoux, J. C. 1975, *Solar Phys.*, **42**, 219.
Holt, S. S. 1974, in *High Energy Quanta in Astrophysics*, ed. F. B. McDonald and C. E. Fichtel (Cambridge: MIT Press), p. 312.
Kane, S. R. 1974, in *IAU Symposium No. 57, Coronal Disturbances*, ed. G. Newkirk (Dordrecht: Reidel), p. 105.
Karzas, W. J., and Latter, R. 1961, *Ap. J. Suppl.*, **6**, 167.
Klein, O., and Nishina, Y. 1929, *Zs. Phys.*, **52**, 853.
Langer, S. H., and Petrosian, V. 1977, *Ap. J.*, **215**, 666.
McMaster, W. H. 1961, *Rev. Mod. Phys.*, **33**, 8.
Nakada, M. P., Neupert, W. M., and Thomas, R. J. 1974, *Solar Phys.*, **37**, 429.
Petrosian, V. 1973, *Ap. J.*, **186**, 291.
Santangelo, N., Horstman, H., and Horstman-Moretti, E. 1973, *Solar Phys.*, **29**, 143.
Tindo, P. I., Ivanov, V. D., Mandel'stam, S. L., and Shuryghin, A. I. 1970, *Solar Phys.*, **14**, 204.
———. 1972*a*, *Solar Phys.*, **24**, 429.
Tindo, I. P., Ivanov, V. D., Valnicek, B., and Livshits, M. A. 1972*b*, *Solar Phys.*, **27**, 426.
Tindo, I. P., Mandel'stam, S. L., and Suryghin, A. I. 1973, *Solar Phys.*, **32**, 469.
Tomblin, F. F. 1972, *Ap. J.*, **171**, 377.
Withbroe, G. L. 1971, *The Menzel Symposium* (NBS Special Pub. 353).

T. Bai and R. Ramaty: Code 660, Laboratory for High Energy Astrophysics, NASA/Goddard Space Flight Center, Greenbelt, MD 20771